ORIGINAL PAPER

Hydrological extreme variability in the headwater of Tarim River: links with atmospheric teleconnection and regional climate

Huaijun Wang · Yaning Chen · Weihong Li

Abstract Variability and possible relationship between monthly 1-day maximum/minimum flow from headwater of Tarim River basin, climatic indices and regional climate were detected by Mann–Kendall test, continuous wavelet transform, cross-wavelet and wavelet coherence methods. The results showed that: (1) hydrological extremes have increased during past 50 years, and the trends of 1-day minimum flow were larger than that of 1-day maximum flow. The most significant change occurred in winter; (2) the hydrological extremes exhibited significant 1-year period and 0.5-year period along the whole hydrological series; (3) different circulation indices may influence the trends of hydrological extremes in different river. The area of polar vortex in North American (i25) and area of Northern Hemisphere polar vortex (i5) showed most significant correlation with 1-day maximum flow and 1-day minimum flow in Aksu River, respectively. In Hotan River, the most significant correlated climate indices with 1-day maximum and minimum flow were Southern oscillation index and area of Northern American Subtropical High (i15), respectively. The area of polar vortex in Atlantic and Europe Sector (i35) showed significant relationships with 1-day minimum flow in Yarkand River; (4) regions of shared power at 0.8–1.5 year mode were found between selected climate indices and the hydrological extremes, anti-phase relations were detected for most of the series;

(5) the fluctuations of temperature have strong effects on hydrological extremes, and significant coherence between regional climate and extremes was found at 0.7–1.5 year scale. The results of the study provide valuable information for improving the long-term forecasting of the hydrological extremes using its relationship with climate indices.

Keywords Hydrological extremes · Climate indices · Wavelet analysis · Tarim River

1 Introduction

There is a broad agreement in the international scientific community that global climate change will alter the frequency and magnitudes of hydrological extremes. A warming climate will enhanced hydrological cycle, and in turn produce more hydrological extremes, such as floods and droughts (Cunderlik and Simonovic 2005a; Zhang et al. 2011). Climate models and hydrological studies also suggested that extreme events are likely to change with global warming (Burn et al. 2010; Taye et al. 2011; Cunderlik and Simonovic 2005b). Extreme runoff will pose serious risks to human life and entail substantial socio-economic and environmental damages (Biggs and Atkinson 2011). In addition, reliable estimates and predictions of extremes runoff characteristics like magnitudes and frequency of floods and droughts are required for water resources management and engineering. Therefore, improving the predictions of extreme runoff characteristics has become one of the major objectives of modern hydrology (Kumar et al. 2010).

The potential impacts of climate change on hydrological extremes have received considerable attention from hydrologists during the last decade. Many studies suggest that

H. Wang · Y. Chen (✉) · W. Li
State Key Laboratory of Desert and Oasis Ecology, Xinjiang Institute of Ecology and Geography, Chinese Academy of Sciences (CAS), Ürümqi 830011, Xinjiang, China
e-mail: chenyn@ms.xjb.ac.cn

H. Wang
University of Chinese Academy of Sciences, Beijing 10049, China

the global warming will increase the frequency and magnitude of extreme hydrological events. Taye et al. (2011) found that climate change will cause the increasing mean runoff and extreme peaks for Nyando catchment for the 2050s. Cunderlik and Simonovic (2005a, b) assessed the potential impact of a changed climate on the timing and magnitude of hydrological extremes in a density populated and urbanized river basin in Southwestern Ontario, Canada and showed that future maximum river flows in the study area will be less extreme. Large-scale patterns of atmospheric circulation determine the distributions of surface temperature and precipitation over land surface, which in turn control key components (e.g. streamflow) of the hydrological cycle (Mishra et al. 2011). Significant research has focused on identifying atmospheric-oceanic climate phenomenon, such as North Atlantic oscillation (NAO) (Pociask-Karteczka et al. 2003), El Nino-Southern Oscillation (ENSO) (Hallack-Alegria et al. 2012; Keener et al. 2010), Pacific Decadal Oscillation (PDO) (Labat 2010), and NAO (Wu et al. 2012). Labat (2008) provided a wavelet-based global analysis of 55 larger river discharge fluctuations located on the five continents and identified statistically significant bands of intermittent fluctuations from interannual 5–8 to decadal, 12–15-year bidecadal, 28-year fluctuations and 40–70-year considering the longest time series available in Europe and North America. Labat (2006, 2010) highlighted an intermittent multiannual variability (4–8, 14–16 and 20–25-year fluctuations) and a persistent multidecadal 30–40-year variability in the global freshwater discharge. Several studies have detected the trends of hydroclimatic variables including annual precipitation, air temperature and runoff time series in the Tarim River basin (Chen et al. 2007; Liu et al. 2011; Liu et al. 2010; Xu et al. 2010b; Zhang et al. 2010). These studies showed that mean annual air temperature, precipitation and streamflow in the headwater of Tarim River experienced an increasing trend. However, the hydrologic extremes and their teleconnection have not been studied. Identifying the affected circulation indices to streamflow is very important for us to predict the occurrence of the hydrologic extremes because of the complex regional terrain environment and atmospheric circulation structure in the arid region of China.

This study uses the wavelet transform approach, the cross-wavelet power and wavelet coherence method to detect the relations between hydrological extremes and circulation indices. The objectives of this study are: (1) to describe changes of hydrological extremes in the headwater of Tarim River; (2) to select the circulation indices which may affect the hydrologic extremes; (3) to apply cross-wavelet and coherence analysis for exploring possible changes in teleconnections as well as the dominant modes in terms of significant power between circulation indices and extremes; (4) to reveal the relationship between regional climate and hydrological extremes.

2 Study area, data and methods

2.1 Study area

The Tarim River basin, located between 73–97°E and 34–45°N, is the largest inland river basin in China, with an area of 1.02×10^6 km^2 (Fig. 1). In its history, the Tarim River basin is composed of 114 rivers of 9 water systems. But now, only three water systems have a natural hydraulic relationship with the mainstream-Aksu River, Hotan River, and Yarkand River. The mean annual natural runoff of surface water is 3.98×10^{10} m^3, which is supplied by water converted from ice and snow and precipitation in the mountains. Among these three headstream flows, Aksu River is the mainstream of the Tarim River, accounting for 73.2 % of the total; the Hotan River and Yerkand River account for 23.2 and 3.6 %, respectively (Chen et al. 2007).

The headwater of the Tarim River Basin, with an area of 36,200 km^2, combines the typical topography of the high mountains and low plain regions. Mean annual precipitation of the mountainous region is more than 300 mm and 70 % of it occurs in the period from June to October, while it varies from 60 to 200 mm over the lower plain regions. The annual air temperature shows intra-annual variations, and the mean is about 8.8 °C. Land use is dominated by barren or sparsely vegetated land (56.2 %) and grassland (31.1 %), while the ratio of woodland, cropland, built-up land and water bodies are 1.2, 5.0, 0.2 and 6.3 %, respectively (Liu et al. 2010). The plain region, where annual precipitation is usually lower than 200 mm, does not generate runoff. Runoff is only generated in the mountainous region and is
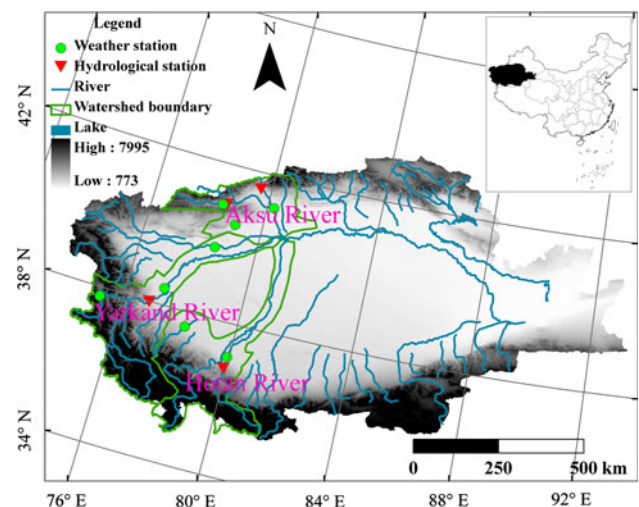

Fig. 1 Distribution of the river system in the Tarim River Basin

consumed in the low plain region by evaporation or irrigation. The streamflow in the headwater sourced from precipitation, glacier, and snow melt and groundwater. Runoff has strong intra-annual variability but lower inter-annual variability.

2.2 Data

Daily hydrological data covering 1960–2007 are collected from four hydrological stations. The hydrological data are provided by the Xinjiang Water Bureau, China. The locations of the hydrological stations can be referred to Fig. 1. The data of Aksu River are the sum of Xehela and Shaliguilank hydrological stations, Yarkand River is reprehensive by Kaqun hydrological station, and Hotan River is reprehensive by Tonguzluok hydrological station. Because all stations are located in the source areas of rivers, so the amount of water less affected by human activities. The missing data are interpolated using the regressive relations between neighboring stations. In our study, we select 1-day maximum flow and 1-day minimum flow to represent the hydrologic extremes in the Tarim River. The homogeneity of the daily streamflow of Tarim River was assessed by the penalized maximal F-(PMF) tests (Wang 2008a, b) through the RH-test software package (Version 3, Wang et al. 2010). Results show that all streamflow time series satisfy the homogeneity.

For circulation indices, the Southern oscillation index (SOI) is used as the ENSO phase indicator, and the monthly data was obtained from Climate Center of China (http://bcc.cma.gov.cn/en/). Similarly, the monthly arctic oscillation (AO) and NAO data were downloaded by the website of the National Weather Service, Climate Prediction Centre of NOAA (http://www.cpc.noaa.gov/data/indices/) for the period January 1954 to December 2007. Other circulation indices, such as Index of the strength of the India–Burma trough (i74) and Index of the area of the northern hemisphere polar vortex (i5), were obtained from the National Climate Centre, China (http://ncc.cma.gov.cn/cn/). This datasets included 74 climate indices, which may affected the climate of China. Because atmospheric circulations and regional conditions are very complex in the headwater of Tarim River, so we have to adopt as much as possible circulation indices to analyze the teleconnection. In this study, we selected a total of 26 circulation indicators which may affected the hydrological variations of Tarim River (Table 1). More information about the selected circulation indices can refer to the book of Zhao (2000).

2.3 Methods

In this study, the nonparametric Mann–Kendall method (Mann 1945; Kendall 1975) is used to detect possible trends in hydrological extremes. In which, the test statistic is given as follows:

$$Z_c = \begin{cases} \dfrac{S-1}{\sqrt{\mathrm{Var}(S)}}, & S > 0 \\ 0, & S = 0 \\ \dfrac{S+1}{\sqrt{\mathrm{Var}(S)}}, & S < 0 \end{cases} \quad (1)$$

where

$$S = \sum_{i=1}^{n-1} \sum_{k=i+1}^{n} \mathrm{sgn}(x_k - x_i) \quad (2)$$

$$\mathrm{sgn}(\theta) = \begin{cases} 1, & \theta > 0 \\ 0, & \theta = 0 \\ -1, & \theta < 0 \end{cases} \quad (3)$$

$$\mathrm{var}[S] = \left[n(n-1)(2n+5) - \sum_t t(t-1)(2t+5) \right] / 18 \quad (4)$$

In which the x_k, x_j are the sequential data value, n is the length of the data set, t is the extent of any given tie. The magnitude of the trend is given as

$$\beta = Median\left(\frac{x_i - x_j}{i - j} \right), \quad \forall j < i \quad (5)$$

In which $1 < j < i < n$. A positive value of β indicates an 'upward trend', and a negative value of β indicates a 'downward trend'. The results of the M–K test are heavily affected by serial correlation of the time serial correlation, so we adopt Yue and Pilon method (Yue et al. 2002) to remove the serial correlation.

Wavelet transforms expand time series into time frequency space and therefore find localized intermittent periodicities. Wavelet analysis can also reveal the localized time and frequency information without requiring the time series to be stationary (Xu et al. 2010a). A continuous wavelet function (CWT) is described from a single function φ by translations and dilations:

$$\phi_{a,b}(t) = |a|^{-\frac{1}{2}} \phi\left(\frac{t-b}{a} \right), \quad a, b \in R \quad (6)$$

where a is the scale parameter, b is the position parameter and t denotes time. The CWT of the signal $f(t)$ with the analyzing wavelet ϕ is the convolution of $f(t)$ with a set of scaled and translated wavelets:

$$W_f(a,b) = \langle f(t), \phi_{a,b} \rangle = |a|^{-\frac{1}{2}} \int_R f(t) \phi * \left(\frac{t-b}{a} \right) dt \quad (7)$$

where * indicate the complex conjugate and $W_f(a,b)$ denotes the wavelet coefficient. Thus concept of frequency

Table 1 Selected circulation indices in this study

Indices	Description
i3	Index of the area of the Northern Hemisphere subtropical high (5E–360E)
i5	Index of the area of the northern hemisphere polar vortex (5 region, 0–360)
i8	Index of the station of the polar vortex center in northern hemisphere (JW)
i12	Index of the strength of the subtropical high over the North African-Atlantic and North American (110W–60E)
i14	The ridge line of the North African subtropical high (20W–60E)
i15	Index of the area of the North African subtropical high (20W–60E)
i17	Index of the northern extend of the North America-Atlantic subtropical high (110W–20W)
i19	Index of the area of the North America-Atlantic subtropical high (110W–20W)
i23	Index of the area of the North American subtropical high (110W–60W)
i25	Index of the area of the polar vortex in the north American (3 region, 120W–30W)
i26	Index of the strength of the polar vortex in the north American (3 region, 120W–30W)
i32	Atlantic and Europe pattern C
i35	Index of the area of the polar vortex in the Atlantic and Europe sector (4region, 30W–60E)
i36	Index of the strength of the polar vortex in the Atlantic and Europe sector (region, 30W–60E)
i40	Index of the area of the subtropical high over the eastern Pacific (175W–115W)
i48	Index of the area of the subtropical high over the South China Sea (100E–120E)
i54	Index of the area of the subtropical high over the Pacific (110E–115W)
i60	Tibetan Plateau (30N–40N, 75E–105E)
i63	Index of the area of the subtropical high over the western Pacific (110E–180E)
i65	Index of the western extend of subtropical high over the Western Pacific
i67	Index of the area of the polar vortex in the Asia (1 region, 60E–150E)
i68	Index of the strength of the polar vortex in the Asia (1region, 60E–150E)
i74	Index of the strength of the India–Burma trough (15N–20N, 80E–100E)
SOI	Southern oscillation index
AO	Arctic oscillation
NAO	North Atlantic oscillation

is replaced by that of scale, which can characterize the variation in the signal, $f(t)$, at a given time scale. The choice of wavelet ϕ depends on the signal to be analyzed. In this case, we select the Morlet wavelet as ϕ. The Morlet wavelet is defined by

$$\phi(t) = \pi^{-1/4} e^{i\omega_0 t} e^{(-t^2/2)} \tag{8}$$

where ω_0 is the non-dimensional frequency (usually taken to be 6 to satisfy the admissibility). The relation between scale a and period T of the Morlet wavelet are given as:

$$T = \frac{4\pi a}{\omega_0 + \sqrt{2 + \omega_0^2}} \approx 1.033a \tag{9}$$

So the Morlet wavelet (with $\omega_0 = 6$) the Fourier period (T) is almost equal to the scale (a).

The wavelet variance that is used to detect the periods present as the power density at different time scale a, which calculated by:

$$E_a = \frac{1}{N} \sum_{b=1}^{N} |W_f(a,b)|^2 \tag{10}$$

where N is the length of data. The cone of influence (COI) is the region of the wavelet spectrum in which edge effects become important. It is defined here as the e-folding time for the autocorrelation of the wavelet power at each scale. Here, COI is used to ignore the edge effects. The significance of the global wavelet spectrum is using red noise model with comparing with the theoretical global wavelet power spectrum.

The cross wavelet transform (XWT) of two series x_n and y_n is defined as

$$W^{XY} = W^X W^{Y*} \tag{11}$$

where * denotes complex conjugation. The cross wavelet power as $|W^{XY}|$. The complex argument $\arg(W^{XY})$ can be interpreted as the local relative phase between x_n and y_n in time frequency space. Circular mean of the phase over regions with higher than 5 % statistical significant that are outside the COI to quantify the phase relationship. The circular mean of a set of $angles(a_i, i = 1, \ldots, n)$ is defined as:

$$a_m = \arg(X,Y) \quad \text{with } X = \sum_{i=1}^{n} \cos(a_i) \quad \text{and} \quad Y = \sum_{i=1}^{n} \sin(a_i) \tag{12}$$

It is difficult to calculate the confidence interval of the mean angle reliably since the phase angles are not independent. The number of angles used in the calculation can be set arbitrarily high simply by increasing the scale resolution. However, it is interesting to know the scatter of angles around the mean. For this the circular standard deviation defined as $s = \sqrt{-2\ln(R/n)}$, where $R = \sqrt{X^2 + Y^2}$. The XWT phase angle within the 5 % significant regions and outside the COI has the mean phase $-176 \pm 12°$ (where $\pm$ designates the circular standard deviation).

Cross wavelet power reveals areas with high common power. Another useful measure is how coherent the cross wavelet transform is in time frequency space. Following the Torrence and Compo (1998) we define the wavelet coherence of two time series as

$$R_R^2(s) = \frac{\left| S\left(s^{-1} W_n^{XY}(s)\right) \right|}{S\left(s^{-1} W_n^X(s)\right) \cdot S\left(s^{-1} W_n^Y(s)\right)} \quad (13)$$

where S is a smoothing operator. The smoothing operator S as

$$S(W) = S_{scale}(S_{time}(W_n(s))) \quad (14)$$

The statistical significance level of the wavelet coherence is estimated using Monte Carlo methods. The Monte Carlo estimation of the significance level requires of the order of 1,000 surrogate data set pairs. The number of scales per octave should be high enough to capture the rectangle shape of the scale smoothing operator while minimizing computing time. Empirically we set 12 scales per octave to be satisfactory.

3 Results

3.1 Trends of hydrological extremes

Monthly hydrological extremes showed increased trends for three rivers (Fig. 2). The summer months exhibited larger increasing magnitudes, while the most significant changes were observed in winter months. For 1-day maximum flow, months from October to February showed significant change in the headwater of Tarim River. While for 1-day minimum flow, there were more months showing significant trends compared with 1-day maximum flow. Months from October to March all demonstrated significant changes. Among three rivers, the Aksu River exhibited most significant changes with more monthly extremes having significant increasing trends. The annual extremes also exhibit significant increasing trends except for 1-day maximum flow in Hotan River (not shown). There were continually increasing trend for 1-day minimum flow, while 1-day maximum flow had a fluctuating increase during study period.

The continuous wavelet transform (CWT) of the monthly hydrological extremes was shown in Fig. 3. All series have higher power in the 1-year band for the whole period, although the power of 1-day minimum flow for Hotan River and Yarkand River was not above the 5 % significant level in some years. The wavelet power spectrum also showed higher power in the 0.5-year bands in all hydrological extreme series. The wavelet variances (not shown) also clearly showed that the pronounced 1-year

period dominated the whole monthly hydrological extreme series. Furthermore, significant 0.5-year period also have distributed along the whole runoff series.

3.2 Correlations between hydrological extremes and circulation indices

The relationships between hydrological extremes and climate indices were explored by using Pearson correlation (Vicente-Serrano et al. 2012; Wang et al. 2013). The correlations calculated were tested for statistically validity at the 95 % significance level. There are many circulation indices having significant correlations with hydrological extremes (Fig. 4; Table 2). 9 Indices and 14 indices showed significant correlation with 1-day maximum flow and 1-day minimum flow in Aksu River, respectively. 12 Climate indices and 19 climate indices have significant relation with 1-day minimum flow in the Yarkand River and Hotan River. For 1-day maximum flow, no indices showed significant correlation with Yarkand River. While for Hotan River, only SOI showed significant correlation with 1-day maximum flow. It is difficult for us to analyze relationships between hydrological extremes and circulation indices using cross-wavelet transform (XWT) and wavelet coherence analysis (WTC), so we only select the climate indices showing most significant correlation with hydrological extremes for next analysis. The i25 and i5 showed most significant correlations with 1-day maximum flow and 1-day minimum flow in the Aksu River, i74 and i35 showing the most significant influence on 1-day maximum flow and 1-day minimum flow in Yarkand River, while for Hotan River, the indices of SOI and i15 were selected, respectively (Table 2). Although so many climate indices significantly correlated with hydrological extremes, there were cross-correlations between each climate indices (Fig. 4). So the most significant correlation indices we selected can represent other indices to a certain extent.

3.3 XWT and WTC analysis between extremes and selected circulation indices

3.3.1 Aksu River

The cross-wavelet transform between i25 and 1-day maximum flow (Fig. 5) showed that significant shared power was observed at 0.8–1.1 year period for the whole study time, and anti-phase relationship was found for those two time series. The same patterns of shared power, phase, and 0.8–1.1 year periodicity were seen in the cross-wavelet transform between i5 and 1-day minimum flow. A more accurate method of analysis by wavelet coherence (WTC), gives a quantity between 0 and 1, and is able to find significant coherence even when the common power of the
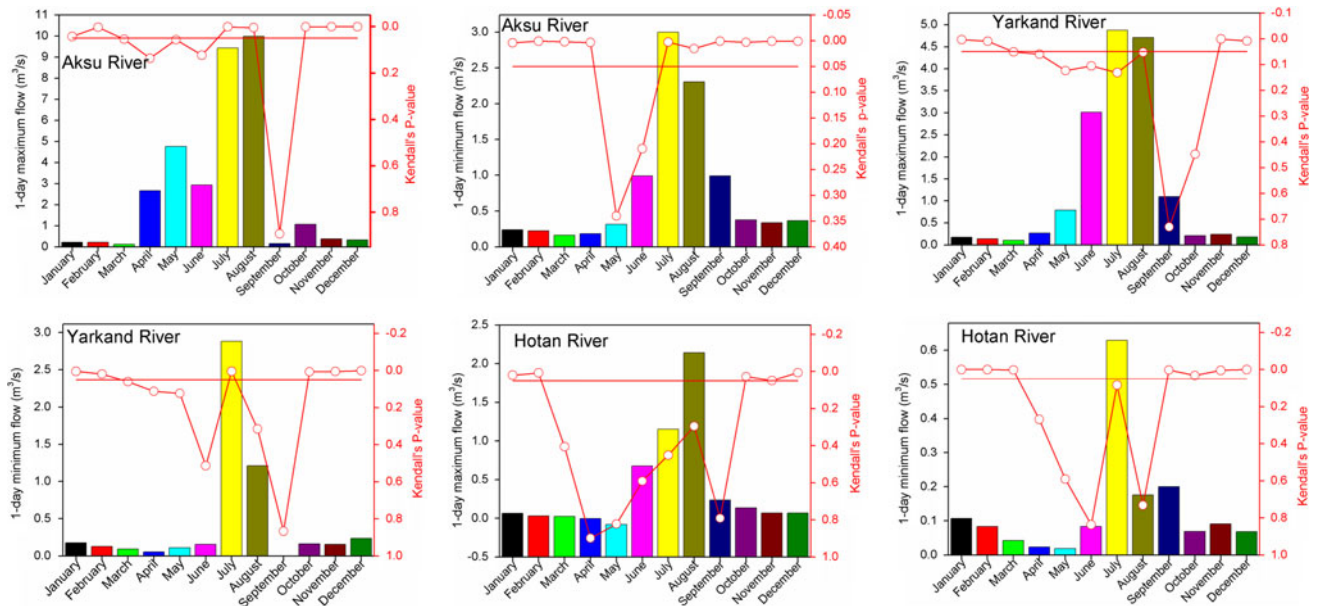
Fig. 2 Trends of monthly extremes for 1-day maximum and 1-day minimum flow (*red circle* the *P* value of Kendall's statistical; *red line*: 0.05 significance level). (Color figure online)

Fig. 3 The continuous wavelet power spectrum of 1-day minimum and 1-day maximum (*left*) and 1-day minimum flow (*right*). The thick contour designates the 5 % significance level against *red* noise and the cone of influence (COI) where edge effects might distort the picture is shown as a *lighter shade*. (Color figure online)
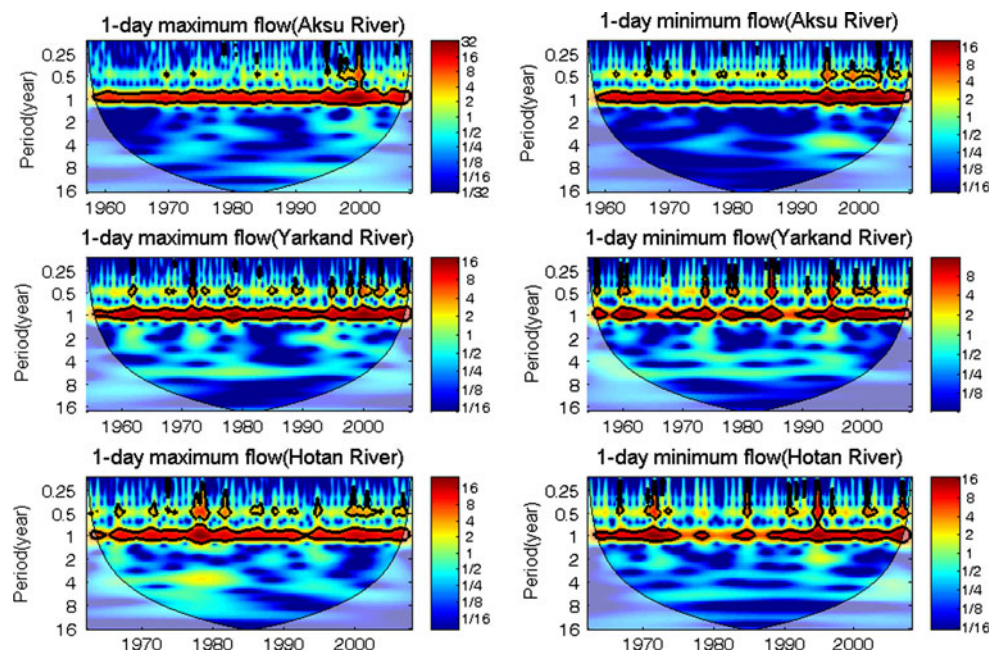
two series is low. Figure 5 illustrated, for the relationship between i25 and 1-day maximum flow, the entire duration of the 0.7- to 1.8-year interval was on average greater than 0.85, and anti-phase relationship also were found for those two time series. During the interval (4–8 year period), there was a higher correlation during 1975–2000 between i25 and 1-day maximum flow. The WTC pattern between i5 and 1-day minimum flow was same as pattern between i25 and 1-day maximum flow, and anti-phase relationship was observed at 0.7–1.5 year period for the whole duration.

3.3.2 Yarkand River

Cross wavelet analysis between hydrological extremes and climate indexes are depicted in Fig. 6. The cross wavelet spectrum and wavelet coherence highlighted mainly interannual covariance with i74 and 1-day maximum flow over the 0.3–0.6-year period and 0.7–1.1-year period during 1960–1968 and 1975–1980 and also controlled the 2–4-year variability over the 1965–1985 period. The i35 appeared 0.9–1.1-year variability related to 1-day minimum flow for

Fig. 4 Correlation coefficients between extremes and circulation indices (*left*) and coefficients among each circulation indices (*right*)

Table 2 Climatic indices showing significant correlation with hydrological extremes (the value in the bracket is the correlation coefficient)

	Significant correlation indices
Aksu River	
1-day maximum flow	i25(−0.533), i15(0.439), i5(−0.390), i26(−0.350), i48(0.32), i12 (0.307), i67(−0.305), i3(0.301), i23(0.301)
1-day minimum flow	i5(−0.503), i15(0.473), i35(−0.447), i67(−0.418), −i25(−0.411), i23(0.382), i3(0.368),and i12(0.367) i68(−0.331), i54(0.331), i40(0.328), i36(−0.312), i63(0.308), i32(0.285), and i8(−0.277)
Yarkand River	
1-day maximum flow	i74(−0.237)
1-day minimum flow	i35(−0.528), i5(−0.432), i25(−0.396), i40(0.366), i14(0.347), i67(−0.312), AO(0.305), i23(0.301), i68(−0.294), i74(0.294), i3(0.270), and i36(−0.268)
Hotan River	
1-day maximum flow	SOI(0.312)
1-day minimum flow	i15(0.711), i23(0.675), i67(−0.677), i3(0.660), i12(0.646), i19(0.627), and i5(−0.619)

the whole study time. The wavelet coherence between i35 and 1-day minimum flow also highlighted a 2–4-year variability over the 1995–2005 period. Anti-phase were observed between i35 and 1-day minimum flow.

3.3.3 Hotan River

For 1-day minimum flow, wavelet analysis put in evidence that 0.7–1.1-year variability was mostly significant correlated with i15. A high coherence over the 1-year band was observed between 1-day maximum flow and SOI, but this common power was not significant. So the results of wavelet analysis were in accordance with correlation results. The regions of shared power at 0.8–1.5 year mode were found between selected climate indices and the hydrological extremes, anti-phase relations were detected for most of the series

3.4 Relations with the basin-wide climate

The temperature showed a significant increasing trend for all three basin, which is in accordance with other studies (Chen et al. 2007). For precipitation, three basins in the headwater demonstrated increasing trends, but most of them showed insignificant changes (not shown). The effects of temperature fluctuations on streamflow were minimal when the temperature was less than 15 °C (Fig. 7). But the impact of relatively small fluctuations in temperature (more than 15 °C) were often amplified by a factor of two or more in the headwater of Tarim River Basin. The scatter between temperature and hydrological extremes was best fit by exponential distribution, which also indicated that there were little effects on streamflow when the temperature was less than a threshold. While this effects will amplify when the temperature is larger than this threshold. As expected, correlations were positive for

Fig. 5 Cross wavelet transform (*left*) and wavelet coherence (*right*) of the hydrological extremes and selected time series for Aksu River. The 5 % significance level against red noise is shown as thick contour. The relative phase relationship is shown as arrows (with in-phase pointing right, anti-phase pointing left, and selected circulation indices leading hydrological extremes by 90° pointing straight down)
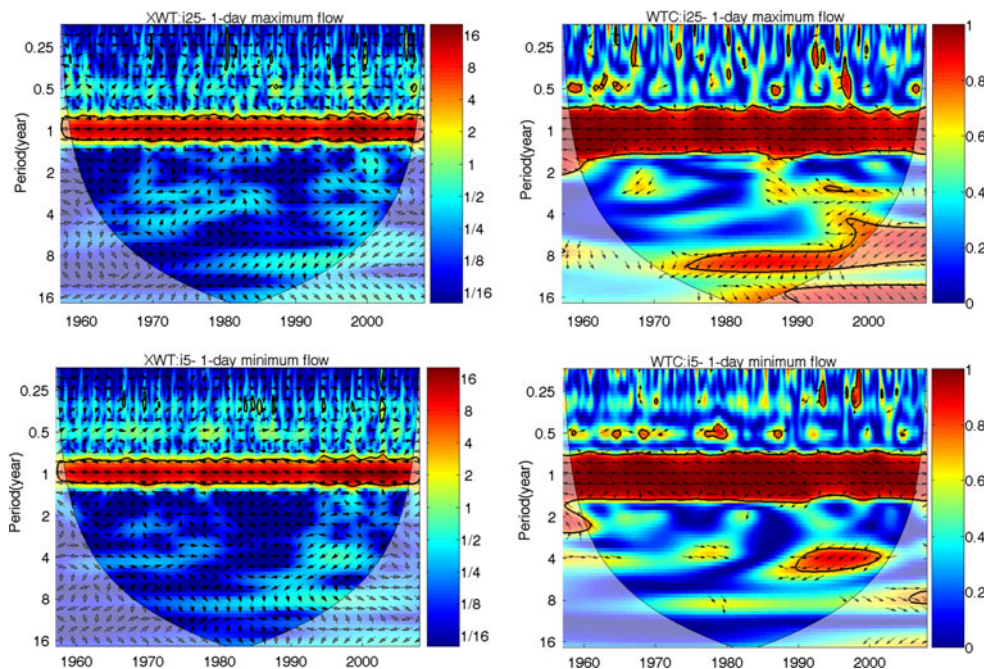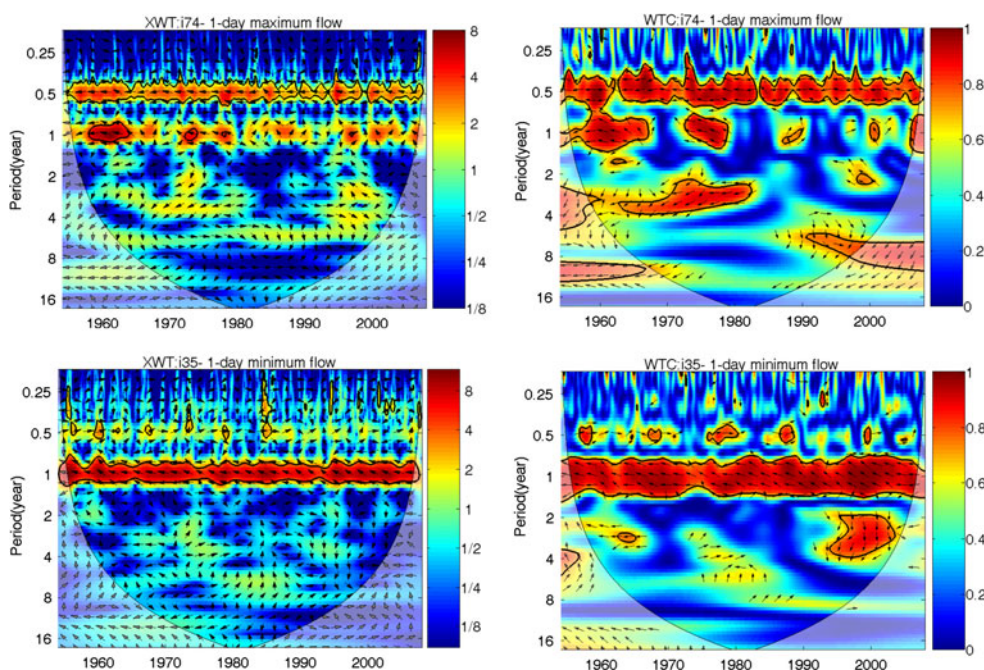
Fig. 6 Same as Fig. 5, but for Yarkand River

precipitation, i.e., an increase leads to an increase in hydrological extremes. The linear fitting between hydrological extremes and precipitation showed a significant positive correlation(F test) between each other, while the Adj. R-square was relatively low. Interesting, higher correlations were found between hydrological extremes and temperature than that between precipitation and hydrological extremes in all three regions. The Adj. R-square between climate variables and 1-day maximum extremes was larger than that of 1-day minimum flow, which

indicted that effects of climate change was severe for 1-day maximum extremes.

Figure 8 shows the wavelet coherence between monthly hydrological extremes and the monthly world-wide precipitation and temperature for Aksu River. The coherence between hydrological extremes and temperature appeared as the most important throughout the spectra at the 0.5–1.7 year period. Phases between temperature and hydrological extremes were almost in phase with each other in all of the significant areas. The Aksu River and
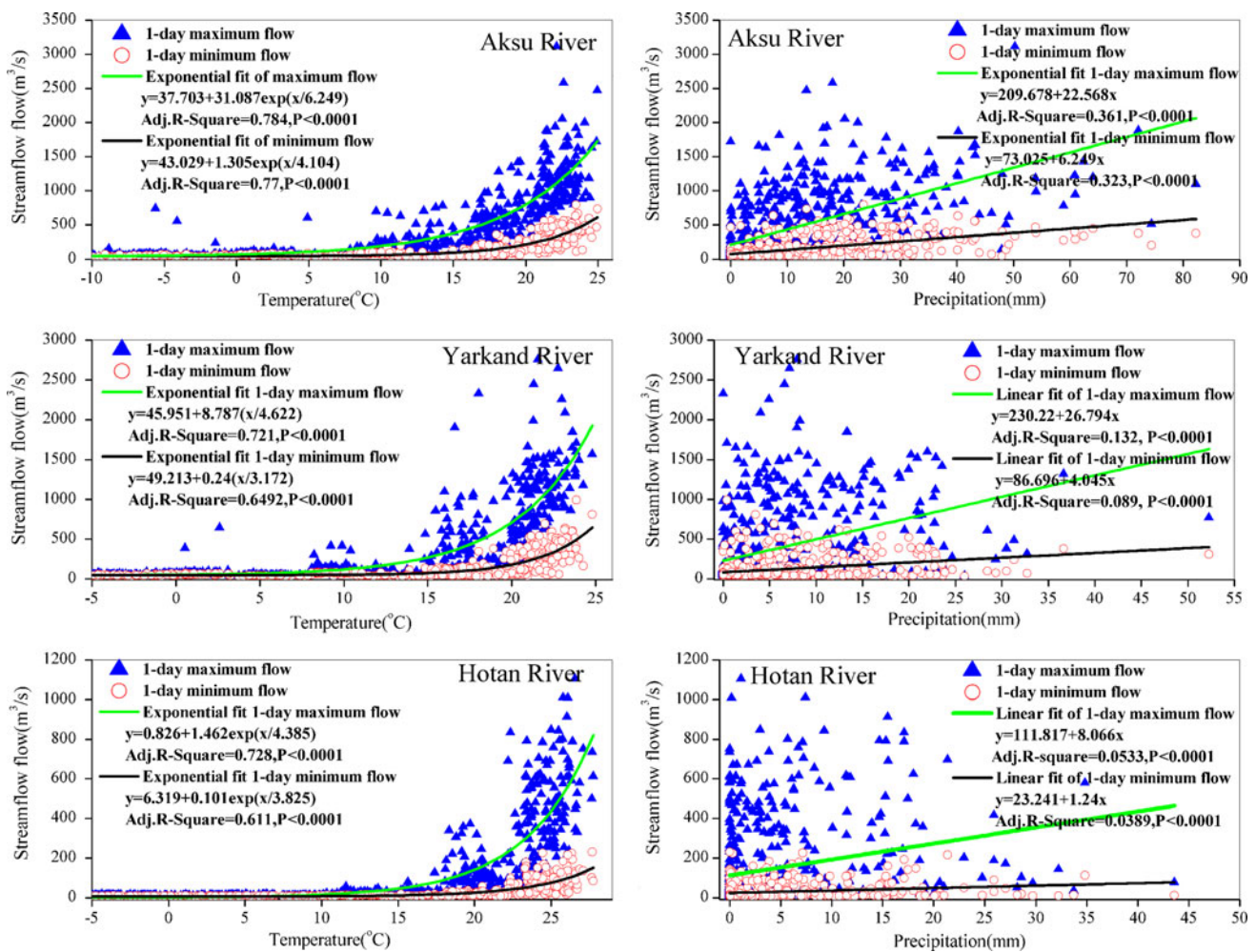
Fig. 7 Relationship between hydrological extremes and regional climate

Yarkand River were the regions where higher than 0.8 coherence coefficients were found across the spectrum for temperature at the 0.7–1.5 year period. Significant coherence between precipitation variability and hydrological extremes was also found at the 0.7–1.5 year scale, but this relationship was not throughout the entire time period. So the effects of temperature were greater than effects caused by precipitation, which is in accordance with regression analysis results.

4 Discussion and conclusions

This paper uses Mann–Kendall test to identify the trends of hydrological extremes. The wavelet analysis is used to qualify the significance of teleconnection between selected climate indices and hydrological extremes in the headwater of Tarim River. The main results are as follows:

(1) Monthly hydrological extremes(1-day maximum flow and 1-day minimum flow)all showed increasing trends during past 50 years, and the most significant changes were found in winter months. The Aksu River showed most significant positive changes, and the trends of 1-day minimum flow were increased greater than that of 1-day maximum flow.

(2) Areas of the highest power for hydrologic extremes were observed in the annual periodicity and sub-annual variability. Higher power were observed in the 1-year band for all extreme time series. The wavelet power spectrum also showed higher power in the 0.5-year bands. So the pronounced 1- and 0.5-year band dominated the whole monthly hydrological extreme series in the headwater of Tarim River basin.

(3) There were many circulation indices having significant correlations with hydrological extremes. The area of polar vortex in North American (i25) and area of Northern Hemisphere polar vortex (i5) have a strong impact on 1-day maximum flow and 1-day minimum flow in the Aksu River, the strength of the India–Burma trough (i74) and the Area of Polar Vortex in Atlantic and Europe Sector (i35) showing
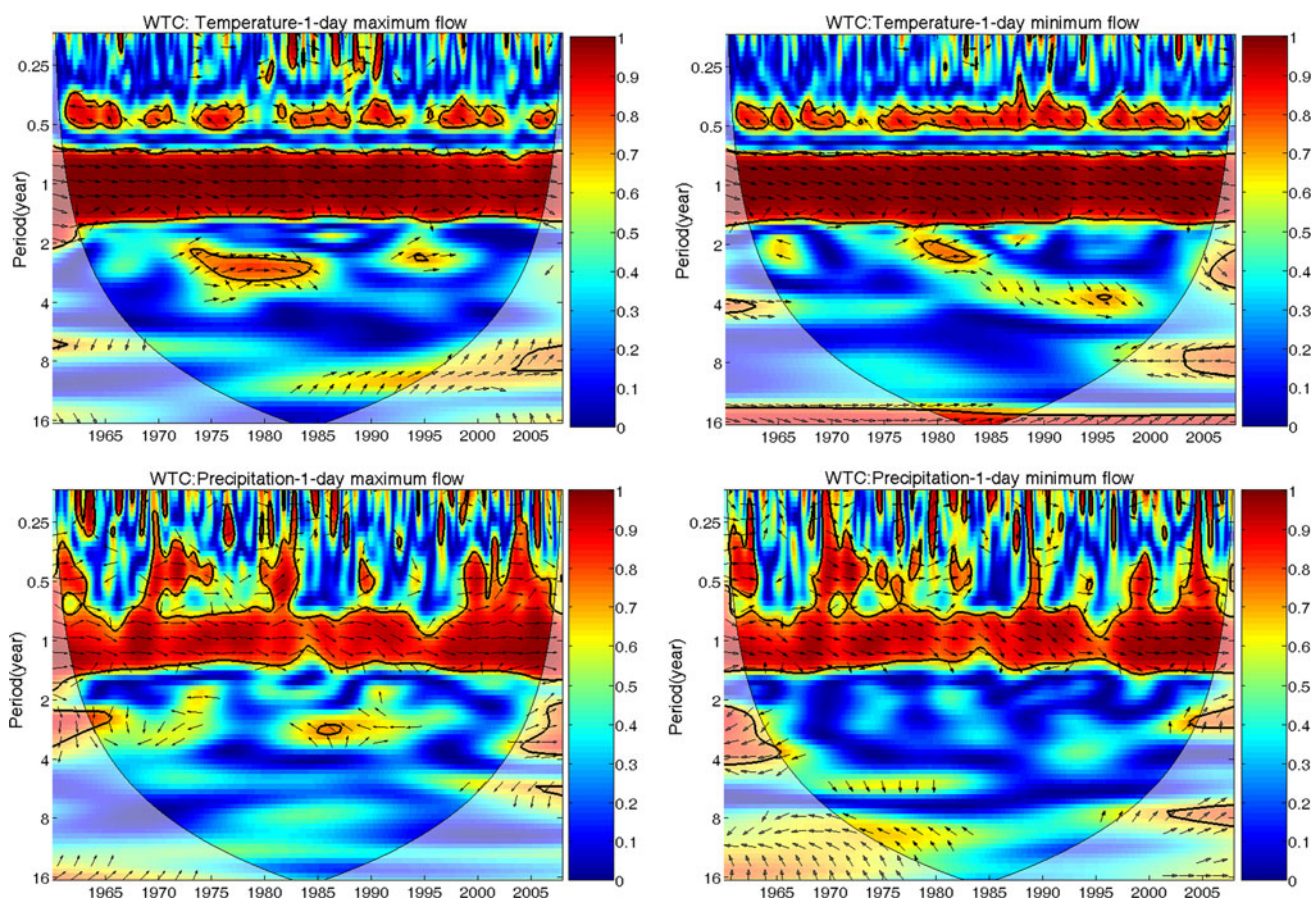
Fig. 8 Wavelet coherence of the hydrological extremes and regional climate in Aksu River

closer relationships with 1-day maximum flow and 1-day minimum flow of Yarkand River, respectively. While for Hotan River, 1-day maximum flow and 1-day minimum flow may influenced by the SOI and area of Northern American Subtropical High (i15).

(4) Regions of shared power were found between selected climate indices and the hydrological extremes. There was common high power and phase in the 0.8–1.5 year mode of variability, and these results confirmed that selected climate indices is causally linked to inter-annual variability of hydrological extremes. The cross-wavelet transform between selected climate extremes and hydrological extremes shows that significant shared power was observed at 0.8–1.1 year period for whole study time series, and significant anti-phase relationship was also observed for these time series. A more accurate method of WTC confirmed the 0.7- to 1.8-year interval for the entire duration between climate indices and hydrological extremes. The hydrological extremes showed high correlation with circulation indices.

(5) The temperature have significant impacted on hydrological extremes. The exponential distribution can best fit the relationship between extremes and temperature. In-phase relationship was observed between extremes and climate variables, and significant coherence was found at 0.7–1.5 year period.

From a new perspective, this paper has provided some conclusions for the response of the runoff process to circulation indices. But due to the complexity of hydro-climatic system coupled with the particularity of the geographical environment, it is difficult to thoroughly understand the nature of hydro-climatic process of the headwater of Tarim River. In fact, the method used in this paper including Mann–Kendall test, wavelet analysis, wavelet cross-correlation, and wavelet coherence are still statistical analysis method, lacing of physical mechanism investigation. Therefore, we sincerely hope that better research methods and results will be proposed to complement insufficient understating the circulation influence on hydrological extremes in the headwater of Tarim River.

References

Biggs EM, Atkinson PM (2011) A characterisation of climate variability and trends in hydrological extremes in the Severn Uplands. Int J Climatol 31(11):1634–1652. doi:10.1002/joc.2176

Burn DH, Sharif M, Zhang K (2010) Detection of trends in hydrological extremes for Canadian watersheds. Hydrol Process 24(13):1781–1790. doi:10.1002/hyp.7625

Chen YN, Li WH, Xu CC, Hao XM (2007) Effects of climate change on water resources in Tarim River Basin, Northwest China. J Environ Sci China 19(4):488–493

Cunderlik JM, Simonovic SP (2005a) Hydrological extremes in a southwestern Ontario river basin under future climate conditions. Hydrol Sci J 50(6):631

Cunderlik JM, Simonovic SP (2005b) Hydrological extremes in a southwestern Ontario river basin under future climate conditions. Hydrol Sci J 50(4):631–654

Hallack-Alegria M, Ramirez-Hernandez J, Watkins DW (2012) ENSO-conditioned rainfall drought frequency analysis in northwest Baja California, Mexico. Int J Climatol 32(6):831–842. doi:10.1002/Joc.2310

Keener VW, Feyereisen GW, Lall U, Jones JW, Bosch DD, Lowrance R (2010) El-Nino/Southern oscillation (ENSO) influences on monthly NO_3 load and concentration, stream flow and precipitation in the Little River Watershed, Tifton, Georgia (GA). J Hydrol 381(3–4):352–363. doi:10.1016/j.jhydrol.2009.12.008

Kendall MG (1975) Rank-correlation measures. Charles Griffin, London, p 202

Kumar R, Samaniego L, Attinger S (2010) The effects of spatial discretization and model parameterization on the prediction of extreme runoff characteristics. J Hydrol 392(1–2):54–69

Labat D (2006) Oscillations in land surface hydrological cycle. Earth Planet Sci Lett 242(1–2):143–154. doi:10.1016/j.epsl.2005.11.057

Labat D (2008) Wavelet analysis of the annual discharge records of the world's largest rivers. Adv Water Resour 31(1):109–117. doi:10.1016/j.advwatres.2007.67.004

Labat D (2010) Cross wavelet analyses of annual continental freshwater discharge and selected climate indices. J Hydrol 385(1–4):269–278. doi:10.1016/j.jhydrol.2010.02.029

Liu Z, Xu Z, Huang J, Charles SP, Fu G (2010) Impacts of climate change on hydrological processes in the headwater catchment of the Tarim River basin, China. Hydrol Process 24(2):196–208. doi:10.1002/hyp.7493

Liu T, Willems P, Pan XL, Bao AM, Chen X, Veroustraete F, Dong QH (2011) Climate change impact on water resource extremes in a headwater region of the Tarim basin in China. Hydrol Earth Syst Sci 15(11):3511–3527. doi:10.5194/hess-15-3511-2011

Mann HB (1945) Non-parametric tests against trend. Econometrica 13:245–259

Mishra AK, Singh VP, Ozger M (2011) Seasonal streamflow extremes in Texas River Basins: uncertainty, trends, and teleconnections. J Geophys Res Atmos 116:D08108. doi:10.1029/2010JD014597

Pociask-Karteczka J, Nieckarz Z, Limanowka D (2003) Prediction of hydrological extremes by air circulation indices. Iahs-Aish, Wallingford, pp 134–141

Taye MT, Ntegeka V, Ogiramoi NP, Willems P (2011) Assessment of climate change impact on hydrological extremes in two source regions of the Nile River Basin. Hydrol Earth Syst Sc 15(1):209–222. doi:10.5194/hess-15-209-2011

Torrence C, Compo GP (1998) A practical guide to wavelet analysis. Bull Am Meteorol Soc 79(1):61–78

Vicente-Serrano SM, Begueria S, Lorenzo-Lacruz J, Camarero JJ, Lopez-Moreno JI, Azorin-Molina C, Revuelto J, Moran-Tejeda E, Sanchez-Lorenzo A (2012) Performance of drought indices for ecological, agricultural, and hydrological applications. Earth Interact 16(10):1–25

Wang XL (2008a) Accounting for autocorrelation in detecting mean shifts in climate data series using the penalized maximal t or F test. J Appl Meteorol Climatol 47(9):2423–2444. doi:10.1175/2008jamc1741.1

Wang XL (2008b) Penalized maximal F test for detecting undocumented mean shift without trend change. J Atmospheric Ocean Technol 25(3):368–384. doi:10.1175/2007jtecha982.1

Wang XL, Chen Hanfeng, Yuehua Wu, Yang Feng PuQ (2010) New techniques for the detection and adjustment of shifts in daily precipitation data series. J Appl Meteorol Climatol 49:2416–2436

Wang HJ, Chen YN, Li WH, Deng HJ (2013) Runoff responses to climate change in arid region of northwestern China during 1960–2010. Chin Geogr Sci 23(3):286–300

Wu Z, Li J, Jiang Z, He J, Zhu X (2012) Possible effects of the North Atlantic oscillation on the strengthening relationship between the East Asian summer monsoon and ENSO. Int J Climatol 32(5):794–800. doi:10.1002/joc.2309

Xu J, Li W, Ji M, Lu F, Dong S (2010a) A comprehensive approach to characterization of the nonlinearity of runoff in the headwaters of the Tarim River, Western China. Hydrol Process 24(2):136–146. doi:10.1002/hyp.7484

Xu ZX, Liu ZF, Fu GB, Chen YN (2010b) Trends of major hydroclimatic variables in the Tarim River basin during the past 50 years. J Arid Environ 74(2):256–267. doi:10.1016/j.jaridenv.2009.08.014

Yue S, Pilon P, Phinney B, Cavadias G (2002) The influence of autocorrelation on the ability to detect trend in hydrological series. Hydrol Process 16(9):1807–1829. doi:10.1002/Hyp.1095

Zhang Q, Xu CY, Tao H, Jiang T, Chen YD (2010) Climate changes and their impacts on water resources in the arid regions: a case study of the Tarim River Basin, China. Stoch Environ Res Risk Assess 24(3):349–358

Zhang Q, Sun P, Chen X, Jiang T (2011) Hydrological extremes in the Poyang Lake Basin, China: changing properties, causes and impacts. Hydrol Process 25(20):3121–3130. doi:10.1002/hyp.8031

Zhao ZG (2000) Summer drought/flood and the environmental field in China. Meteorological Press, Beijing